

Investigation on Carbonizing From Mold Flux into Ultra-low-Carbon Steel During Continuous Casting



QIAN LONG, WANLIN WANG, and KUN DOU

Carbonizing phenomena from carbon-containing mold flux into ultra-low-carbon liquid steel have always been one of the important factors affecting the surface quality of continuous casting billets. An experimental method has been adopted in this investigation to study the carbonizing behavior of mold flux into liquid steel during continuous casting of ultra-low-carbon liquid steel, and the locations where carbonizing occurs during the continuous casting process were predicted by ANSYS Fluent numerical simulations. The results indicate that the low-carbon mold flux with carbon concentration 2.19 pct would form the thickness of steel carbonizing about 1500 μm , and the high-carbon mold flux with carbon concentration 3.64 pct would form the thickness of steel carbonizing over 4000 μm when liquid steel–mold flux contact for 20 seconds at high temperature. And the metallographic structure of primitive ferrite firstly precipitates the chain pearlite ferritic at the ferrite grain boundary and then grows up to form flake pearlite. Furthermore, the numerical simulation results show that the carbonizing phenomenon is likely to occur at a quarter of the width in the thin slab where there are the violent steel liquid free surface fluctuations during the continuous casting process, which is consistent with the locations of carbonizing found in actual production sampling.

<https://doi.org/10.1007/s11663-022-02687-z>

© The Minerals, Metals & Materials Society and ASM International 2022

I. INTRODUCTION

MOLD flux is an indispensable additive in the continuous casting process of liquid steel. It can (1) provide thermal insulation and isolate the air to prevent the initial solidification shell and liquid steel from being oxidized,^[1] (2) absorb the inclusions in the liquid steel to improve its purity,^[2,3] (3) forming a molten mold flux film between the liquid steel and mold provides lubrication to ensure continuous casting, and (4) improve heat transfer between the molten steel and the mold^[4,5]; thus ensuring normal billet drawing progress and obtaining high-quality cast billets.^[6,7] Carbon is an absolutely necessary additive in mold flux during continuous casting. Adding a certain amount of carbon can effectively adjust the melting characteristics of mold flux, improve the sinter tendency of mold flux, improve

the thermal insulation performance of the powder mold flux, and control the oxidizing properties of molten mold flux, which can reduce the operational problems and improve the quality of the casting slab.^[8,9]

However, it is very possible that the steel undergoes a carbonizing phenomenon due to the carbon diffuse into liquid steel during continuous casting, especially the high-carbon concentration gradient between the ultra-low-carbon steel and the carbon-containing mold flux. Hence, for ultra-low-carbon steel casting billets, understanding the mechanism of carbonizing from mold flux into liquid steel in the process of mold flux continuous casting is the premise to solving the carbonizing phenomenon. However, the liquid steel–mold flux interface in the continuous casting mold has always been high temperature, the sealing is unobservable, and complex physical and chemical behaviors occur, which is regarded as a “black box.” Therefore, it is necessary to find a suitable experimental method to simulate the liquid–liquid interface behavior of the liquid steel–mold flux interface during continuous casting. Recently, an experimental method for simulating the behavior of mold flux during continuous casting was adopted to investigate the melting and consumption of mold flux.^[10,11] This method can obtain the most typical three-layer structure of mold flux, including a granular mold flux layer, a sinter mold flux layer, and a molten mold flux. In particular, the contacting liquid–liquid

QIAN LONG, WANLIN WANG, and KUN DOU are with the School of Metallurgy and Environment, Central South University, Changsha 410083, Hunan, P.R. China and also with the National Center for International Research of Clean Metallurgy, Central South University, Changsha 410083, P.R. China. Contact e-mail: Kun.Dou@csu.edu.cn

Manuscript submitted July 30, 2022; accepted October 30, 2022.

Article published online November 23, 2022.

two-phase interface for steel liquid–molten mold flux at high temperature is reproduced in the laboratory, which can reflect the characteristics of the liquid steel–mold flux interface in the mold during continuous casting. In addition, the liquid level fluctuation generally accelerates the diffusion of carbon in the mold flux to the carbon in the molten steel,^[12] and the violent fluctuation of the liquid surface will cause the carbon-rich layer to be involved in the liquid steel and cause the carbonizing of the liquid steel during continuous casting.^[13,14] The surface of liquid steel in the mold is directly contacting by the mold flux, and the numerical simulation of the transient characteristics of the liquid surface fluctuation can be used as a more accurate auxiliary method to predict the fluctuation of liquid steel during continuous casting.^[15–17]

Therefore, we adopted this simple and reliable experimental method to investigate the three-layer distribution of carbon-containing mold flux in the continuous casting mold after melting and the carbonizing behavior of ultra-low-carbon liquid steel. Here, the melted three-layer structure of mold flux, including molten mold flux, sinter mold flux, and granular mold flux, is investigated. Next, the metallographic structure and carbon distribution characteristics were analyzed, and the carbon concentration distribution from the mold flux–steel interface to the interior of the steel after carbonizing with time and distance was also investigated by EPMA (JXA-8230 Electron Probe Micro Analysis), which is discussed by the double-film model within phases and unsteady diffusion in semi-infinite medium. Eventually, the carbonizing location on continuous casting thin slabs is predicated using the software ANSYS Fluent based on actual continuous casting process parameters and mold morphology characteristics.

II. EXPERIMENTAL PROCEDURE

A. Sample Preparation

The main composition of steel sample for commercial ultra-low-carbon steel used in experiment is presented in Table I. The main composition for containing carbon mold flux including both A slag (carbon percentage 2.19 pct) and B slag (carbon percentage 3.64 pct) used with ultra-low-carbon steel during continuous casting is presented in Table II.

B. High-Temperature Melting Test

Prepared the steel sample for an 8.5 * 12 mm cylindrical was put it into a quartz tube with an inner diameter of 9 mm, and then added mold flux with a height of 12 mm on the upper part of the steel sample. The schematic diagram of the melting process of steel–slag is shown in Figure 1. Here, the steel was heated by the induction coil, and the coil power was continuously increased until the observed steel began to melt from the window, and then held power (60 kW) for a certain period of time (10, 20, and 40 seconds)

accompanying steel liquid free surface fluctuation to a certain extent. Obviously, the molten, sinter, and granular layer for mold flux can be obtained. Subsequently, the heating equipment is turned off, and the steel and mold flux are taken out of the furnace body after cooling for further analysis.

C. Carbon Structure and Content Analysis

It was investigated that the amount of molten mold flux layer, sinter mold flux layer, and granular mold flux layer and its carbon weight percentage were determined by the CS-600 carbon and sulfur determinator (LECO Corporation, USA). The steel sample was mounted with resin, and the micro-metallographic structure by optical microscope and carbon concentration distribution with distance and holding time from the mold flux–steel interface to the interior of the steel were investigated by EPMA.

III. RESULTS

A. Melting Behavior of Mold Flux with Steel Liquid Holding Temperature Time

Figure 2 shows the macroscopic interface characteristics between liquid steel and molten mold flux after cooling with different liquid steel holding temperature times for 10, 20, and 40 seconds from left to right. The solid line is the height of mold powder reaching after adding mold flux without heating, and the dotted line is the upper end scale line of the steel sample after heating. Obviously, with the liquid steel holding temperature for a certain period of time, the mold flux will form the three-layer structure, including granular, sinter, and molten layer. From Figure 2(a), with the increase of holding temperature time, the mold flux was continuously melted, and the A slag was almost completely melted at 40 seconds. Similarly, with the increase in holding temperature time, the mold flux was continuously melted from Figure 2(b). However, the melting amount of B slag is obviously less than that of A slag with the same liquid steel holding temperature time, and the change in the amount of continuous melting for B slag after a holding temperature time of 20 seconds is not particularly large, which is due to the carbon effectively reducing the melting rate of the mold flux and isolating the heat transfer between the granular mold flux.^[3,4]

Figure 3 shows the variation of amounts for molten mold flux, sinter mold flux, and granular mold flux layers with liquid steel holding temperature at different times. Obviously, the amount of molten mold flux layer of A slag is higher than that of B slag, which is consistent with the results reported in the literature.^[11] Correspondingly, the amount of the granular mold flux layer of B slag is higher than that of A slag. At the 10 and 20 seconds for liquid steel holding temperature time, the amount of the sinter mold flux layer of A slag is higher than that of B slag, which may be due to the higher melting rate of A slag that causes easier sintering.

Table I. The Main Composition of Steel Sample for Ultra-low-Carbon Steel (Wt Pct)

C	Si	Mn	Al	P	S	O	Fe
0.002	1.100	0.300	0.038	< 0.003	0.018	< 0.003	balance

Table II. The Main Composition of Mold Flux Used in Ultra-low-Carbon Steel During Continuous Casting (Wt Pct)

	R	SiO ₂	CaO	Al ₂ O ₃	MgO	Na ₂ O	K ₂ O	MnO ₂	Fe ₂ O ₃	F	C	Other
A	0.96	35.95	34.64	4.64	4.88	4.08	0.67	2.71	1.35	7.50	2.19	1.39
B	0.96	35.59	34.30	4.59	4.83	4.04	0.66	2.68	2.13	7.43	3.64	0.11

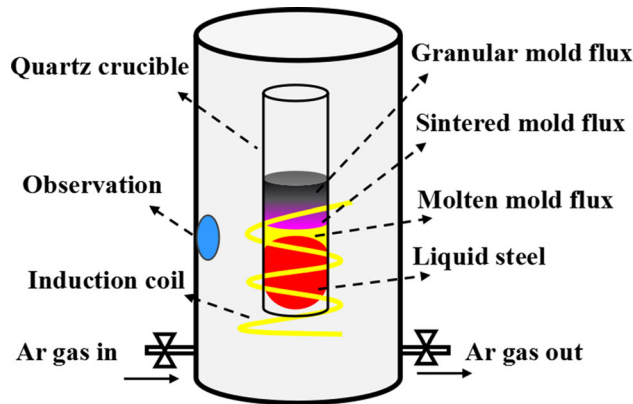


Fig. 1—Schematic diagram of the simulated mold flux carbonizing into liquid steel equipment.

However, the amount of the sinter mold flux layer of A slag becomes thinner at 40 seconds, which may be that the continuous high temperature makes low-carbon mold flux mostly melted completely.

In addition, the carbon concentration of each mold flux layer with the liquid steel holding temperature different time is shown in Table III. Obviously, the carbon concentration of the molten mold flux layer for the A slag is higher than that of the B slag. This may be because the iron oxide content of the B slag is higher than that of the A slag, which causes the higher oxidation of the B slag.^[18] In addition, the carbon concentration in the sinter layer of B slag is higher than that of A slag. The variation of carbon content in the granular layer between A slag and B slag is only 1.49 pct, but the carbon concentration in the sinter layer for B slag is 3.06 to 3.13 pct, and the carbon concentration in sinter layer of A slag is 0.422 to 0.463 pct. This may be that the B slag forming a more rich layer results in a very high-carbon concentration in the sinter layer in high-carbon mold flux.

B. Metallographic Structure of Steel After Carbonizing

Figure 4 shows the typical metallographic structure from the A slag–steel interface to the interior of steel with liquid steel holding temperature time for (a) 10 seconds and (b) 20 seconds. It can be seen that from the slag steel

interface to the interior of steel all are original existing ferrite structure with liquid steel holding temperature time for 10 seconds as shown in Figure 4(a). It can be also seen that the slag–steel interface precipitates the darker chain pearlites structure; however, the interior of steel still is original existing ferrite structure with liquid steel holding temperature time for 20 seconds as shown in Figure 4(b). This indicates that the A slag has generated a carbonizing phenomenon for high-carbon chain pearlite structure with the liquid steel holding temperature time of 20 seconds.

Figure 5 shows the typical metallographic structure from the B slag–steel interface to the interior of steel with liquid steel holding temperature time for (a) 10 seconds and (b) 20 seconds. It can be seen that the slag–steel interface precipitates the darker chain pearlite structure; however, the interior of steel still is original existing ferrite structure with liquid steel holding temperature time for 10 seconds as shown in Figure 5(a). It can be also seen that there are a large number of flake pearlite accounted the most of the whole surface from the slag steel interface to the interior of steel with liquid steel holding temperature time for 20 seconds as shown in Figure 5(b). This indicates that the B slag has generated a carbonizing phenomenon for high-carbon chain pearlite structure with the liquid steel holding temperature time of 10 seconds. Further, the carbon of the chain pearlite regarding the grain boundary could have been diffused to form the flake pearlite with the liquid steel holding temperature for 20 seconds.

C. Distribution Characteristics of Carbon in the Steel After Carbonizing

Figure 6 shows the distribution characteristics of carbon in the steel after carbonizing for (a) A slag–steel interface with liquid steel holding temperature time for 10 seconds, (b) B slag–steel interface with liquid steel holding temperature time for 10 seconds, and (c) B slag–steel interface with liquid steel holding temperature time for 20 seconds. It can be seen that the carbon elements distribute evenly on the entire surface to form ultra-low-carbon ferrite structure with liquid steel holding temperature time for 10 seconds as shown in Figure 6(a). It can also be seen that the carbon elements distribute in the grain boundaries of the ferrite structure

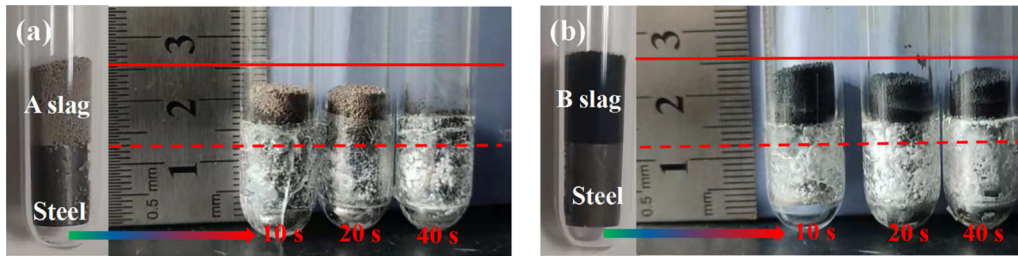


Fig. 2—Macroscopic interface characteristics after cooling between steel and (a) A slag, and (b) B slag with different liquid steel holding temperature times.

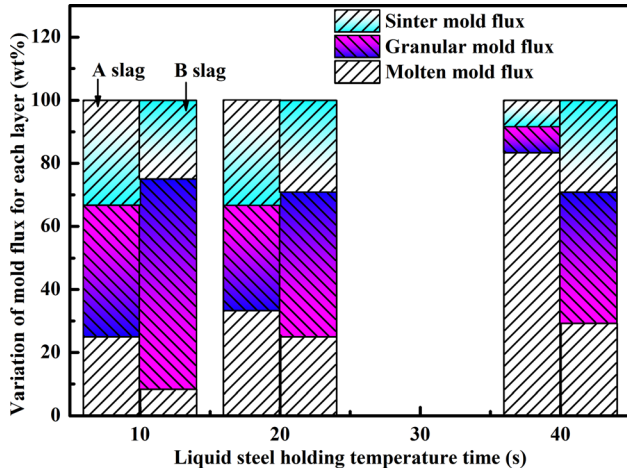


Fig. 3—Variation of amounts for molten mold flux, sinter mold flux, and granular mold flux layers with liquid steel holding temperature at different times.

when ultra-low-carbon steel early takes place carbonizing phenomenon as shown in Figure 6(b); however, the carbon elements evenly distribute on lamellar pearlite structure when ultra-low-carbon steel takes place more serious carbonizing as shown in Figure 6(c). It indicates that the high-carbon structure of steel firstly precipitates from the ultra-low-carbon ferrite grain boundary, and then diffuses and grows to form a flake structure.^[19,20]

In addition, the carbon concentration distribution with distance from the A slag–steel interface to the interior of the steel after carbonizing with liquid steel holding temperature for 10 and 20 seconds was characterized by EPMA as shown in Figure 7. It can be seen that the carbon concentration reduces with increasing the distance from low-carbon mold flux–steel interface to interior of the steel after carbonizing with liquid steel holding temperature time for 10 seconds as shown in Figure 7(a). It can be also seen that the carbon diffusion thickness is about 800 μm , and the maximum carbon concentration is approximately 0.8 pct with liquid steel holding temperature time of 10 seconds. It is known that the carbon weight percentage for ultra-low-carbon steel is only 0.002 pct, and the steel that produces pearlite structure is generally medium and high-carbon steel. Although a part of the molten steel has undergone

Table III. The Carbon Concentration of Each Mold Flux Layer (Wt Pct)

	Granular Mold Flux	Sinter Mold Flux	Molten Mold Flux
A Slag 10	2.19	0.422	0.0239
A Slag 20	2.19	0.463	0.0390
B Slag 10	3.68	3.06	0.0150
B Slag 20	3.68	3.13	0.0100

carbonizing, the amount of carbonizing is not enough to cause the steel to appear pearlite. Additionally, it can be seen that the carbon concentration also reduces with increasing the distance from A slag–steel interface to interior of the steel after carbonizing with liquid steel holding temperature time for 20 seconds as shown in Figure 7(b). It can also be seen that the carbon diffusion thickness is about 1500 μm , and the maximum carbon concentration is approximately 1.2 pct with a liquid steel holding temperature time of 20 seconds.

Furthermore, the carbon concentration distribution with distance from the B slag–steel interface to the interior of the steel after carbonizing with liquid steel holding temperature for 10 and 20 seconds was characterized by EPMA as shown in Figure 8. It can be seen that the carbon concentration reduces with increasing the distance, which is similar with the results from A slag, from B slag–steel interface to interior of the steel after carbonizing with liquid steel holding temperature time for 10 seconds as shown in Figure 8(a). It can also be seen that the carbon diffusion thickness is greater than 2100 μm , and the maximum carbon concentration is approximately 1.2 pct with liquid steel holding temperature time of 10 seconds. Additionally, it can be seen that the carbon concentration evenly distributes with increasing the distance from B slag–steel interface to interior of the steel after carbonizing with liquid steel holding temperature time for 20 seconds as shown in Figure 8(b). It can also be seen that the maximum carbon concentration is approximately 1.0 pct with a liquid steel holding temperature time of 20 seconds. It

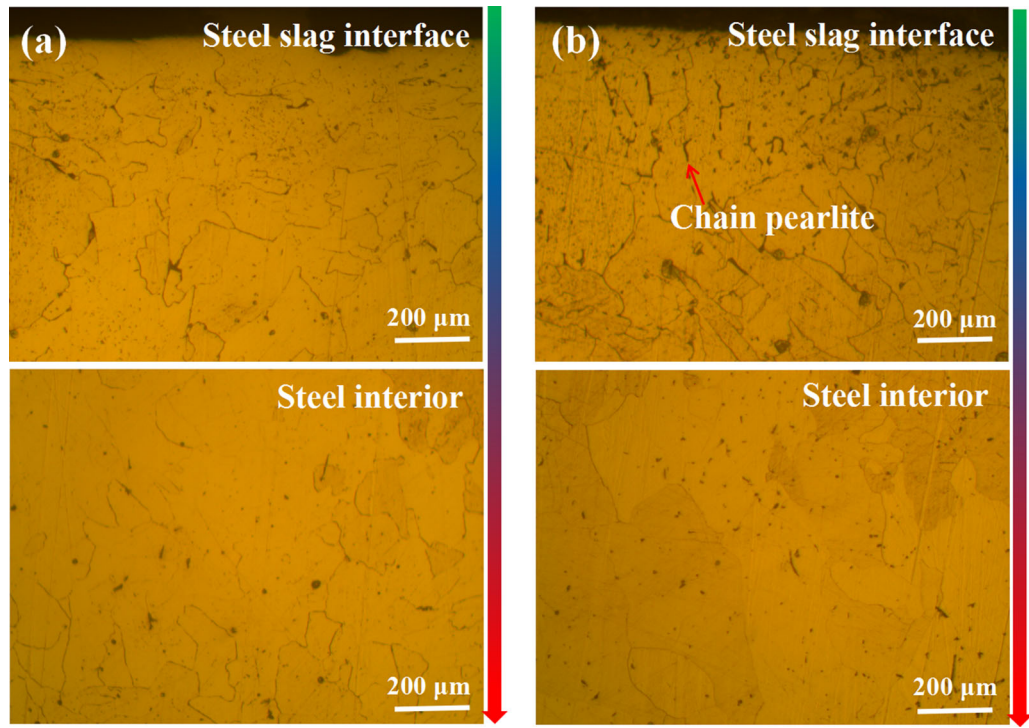


Fig. 4—Typical metallographic structure from the A slag–steel interface to the interior of steel with liquid steel holding temperature time for (a) 10 seconds and (b) 20 seconds.

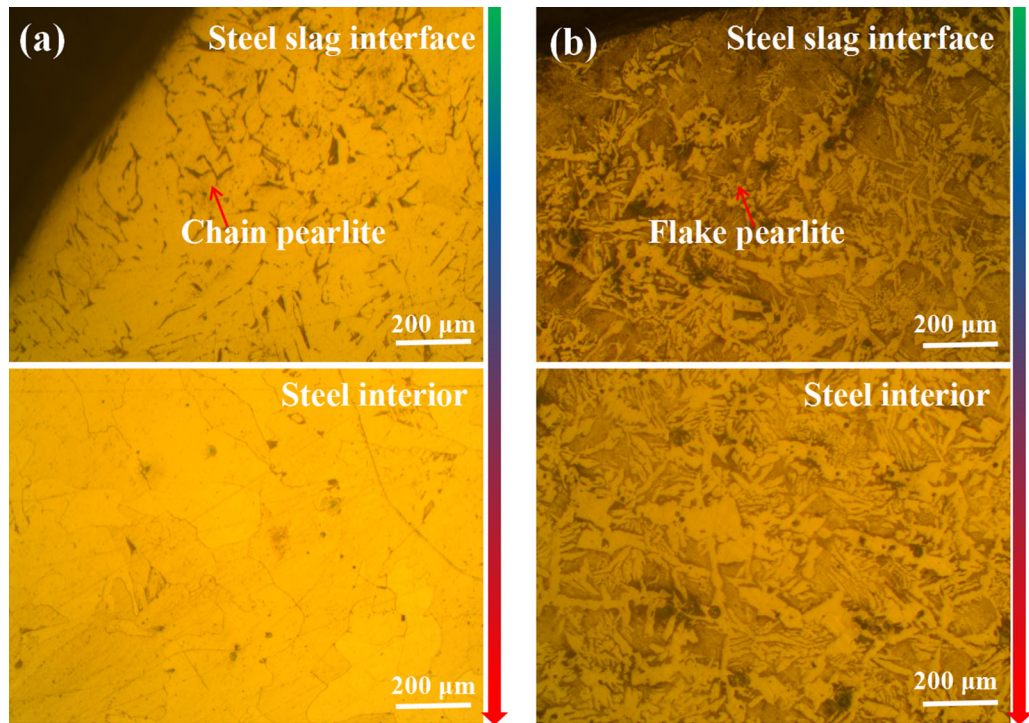


Fig. 5—Typical metallographic structure from the B slag–steel interface to the interior of steel with liquid steel holding temperature time for (a) 10 seconds and (b) 20 seconds.

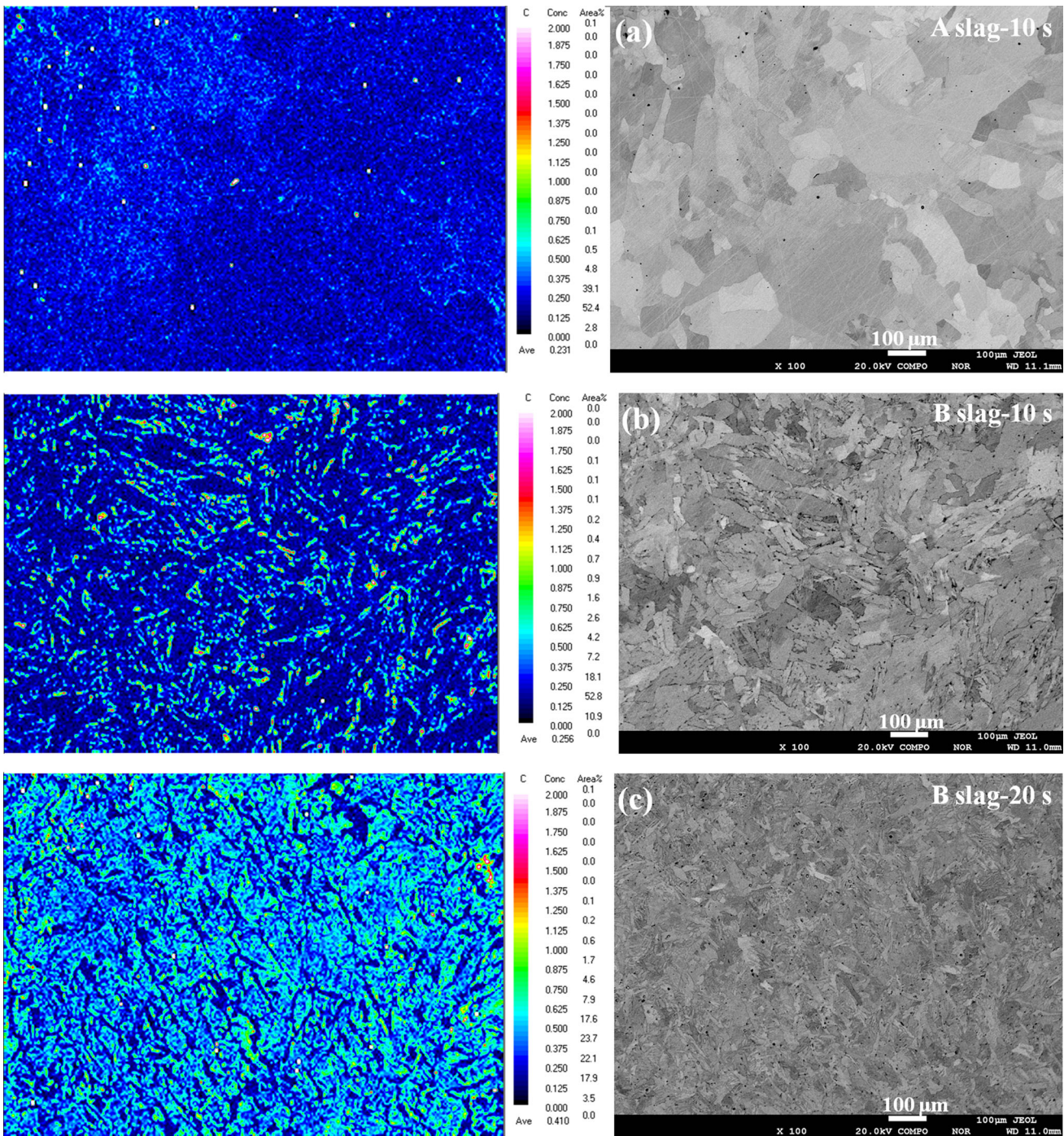


Fig. 6—Distribution characteristics of carbon in the steel after carbonizing for (a) A slag–steel interface with liquid steel holding temperature time for 10 seconds, (b) B slag–steel interface with liquid steel holding temperature time for 10 seconds, and (c) B slag–steel interface with liquid steel holding temperature time for 20 seconds.

was known that the thickness of carbon diffusion has exceeded $4000\ \mu\text{m}$ for whole sample from the metallographic structure of the interior of steel as shown in Figure 5(b). Comparing Figures 7(b) and 8(a), it can be known that the maximum carbon concentration value is almost the same from the A and B slag–steel interface to the interior of steel.

D. Simulation of Liquid Steel Flow Field Distribution and Free Surface Fluctuations

Based on the above analysis, a mathematical model is built to study the fluid flow and surface wave evolution behavior of the liquid steel during the continuous casting process of the steel in the CSP mold region. Three-dimensional Navier–Stokes Equations are solved using the finite volume method in ANSYS Fluent

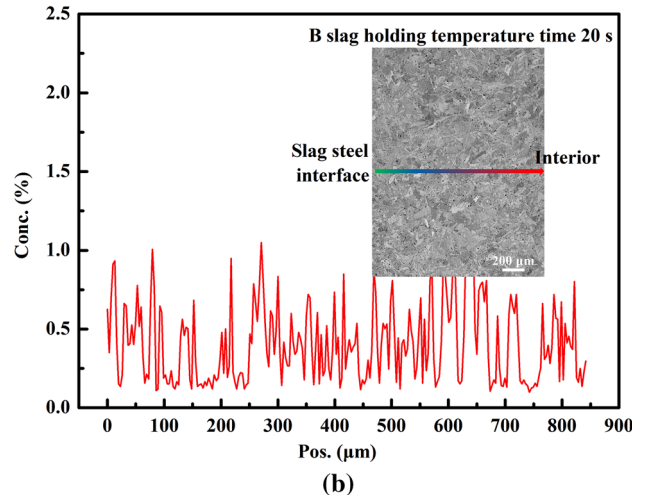
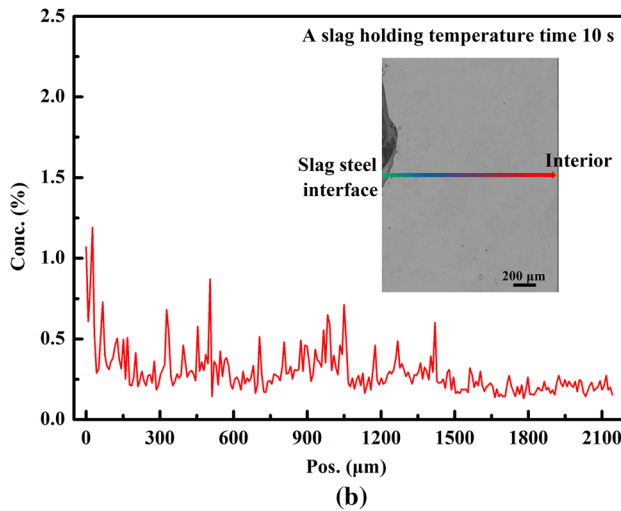
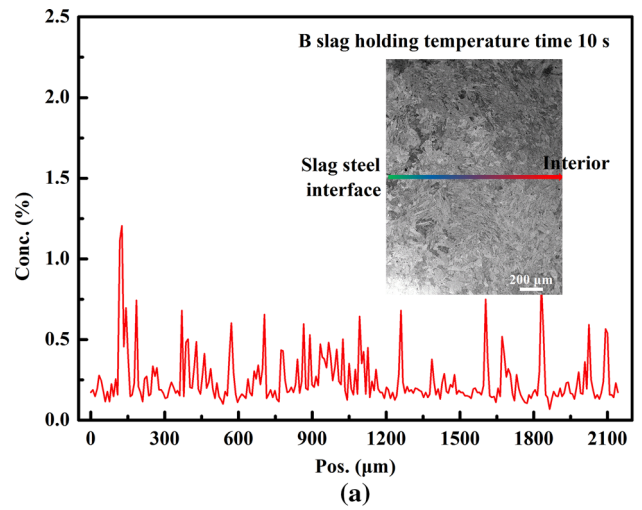
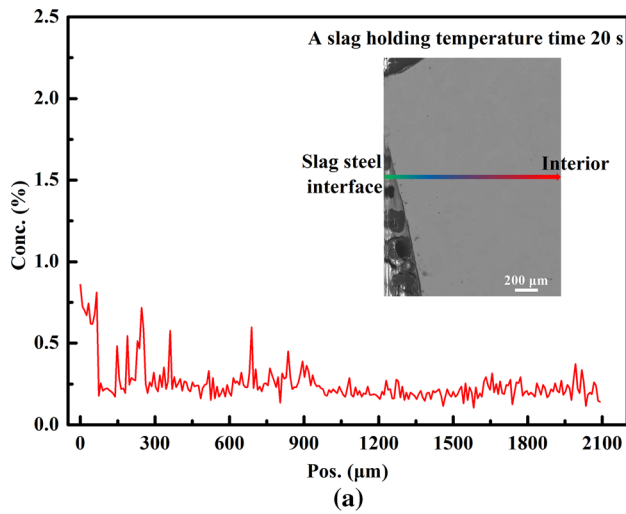


Fig. 7—Carbon concentration distribution from the A slag–steel interface to the interior of the steel after carbonizing with liquid steel holding temperature for (a) 10 seconds and (b) 20 seconds.

Fig. 8—Carbon concentration distribution from the B slag–steel interface to the interior of the steel after carbonizing with liquid steel holding temperature for (a) 10 seconds and (b) 20 seconds.

platform, and the evolution of the steel free surface on the top of the mold is described using the volume of fluid (VOF) method. To model the turbulence in the mold filling process, a low Reynolds number $k-\epsilon$ model is applied. And the roughness of the wall area is described using wall functions, which is compiled using user-defined functions (UDFs) based on C++. Details about the set-up and relevant models used in this work can be found elsewhere.^[21–23] Figure 9 shows the schematic diagram of the computational domain meshed. Here, it has specifically described the coordinates, dimensions, and critical boundary surface. Next, the fluid velocity distribution is displayed by the plane with the X – Y axis as shown in Figure 10, and the fluctuation of the liquid steel free surface is displayed in the Z axis direction as shown in Figure 11.

Figure 10 shows the fluid velocity distribution diagram of liquid steel in the mold with an X -axis dimension of 1200 mm. The liquid steel flows out from the immersion nozzle, and the high-speed streams

impact the four return areas formed after the narrow surface of the mold as shown in Figure 10(b). The liquid steel in the jet area expands continuously during the traveling process and the fluid velocity gradually decreases, and still maintains a certain fluid velocity after reaching a certain depth; the upper recirculation zone is in the area from the edge to 1/4, where the fluid velocity of liquid steel is larger, and the area with the largest fluid velocity of liquid steel at 1/4 is closer to the free surface. Furthermore, Figure 11 shows the simulated fluctuation of the liquid steel free surface in the mold at different times. It can be seen that during the continuous casting process, the liquid steel fluctuates most violently at 1/4 of the width direction of the slab, and the free surface is in a trough position, which easily causes liquid steel to carbonizing as the result of the containing carbon mold flux drawn into liquid steel. Additionally, the fluctuation of the liquid level shows periodic changes. The maximum distance between peak and trough over time is about 10 mm at 1/4 of the width direction of the slab, and the fluctuation period of the free surface is about 6 to 7 seconds.

Figure 12 shows the analysis process of the carbonizing micro structure of a thin slab. The sampling position is at 1/2, 1/4, 1/8 of the distance from the edge to the width direction for thin slab as shown in Figure 12(a); microscopic observation section is the consisting part of thickness and width as shown in Figure 12(b) and the typical carbonizing metallographic structure as shown in Figure 12(c). All samples were corroded by 4 pct nitric acid alcohol, and the carbonizing metallographic structure of pearlite was mainly distributed from the distance of 1/4 to 1/8 from the edge to the width direction for a thin slab. Obviously, the carbonizing position is mainly in the position where the liquid surface fluctuates more violently, considering the above simulation results as shown in Figures 10 and 11.

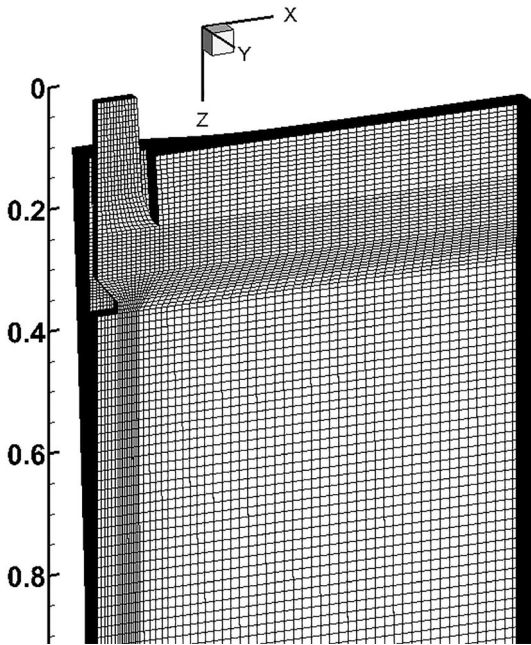


Fig. 9—The schematic diagram of the computational domain meshed.

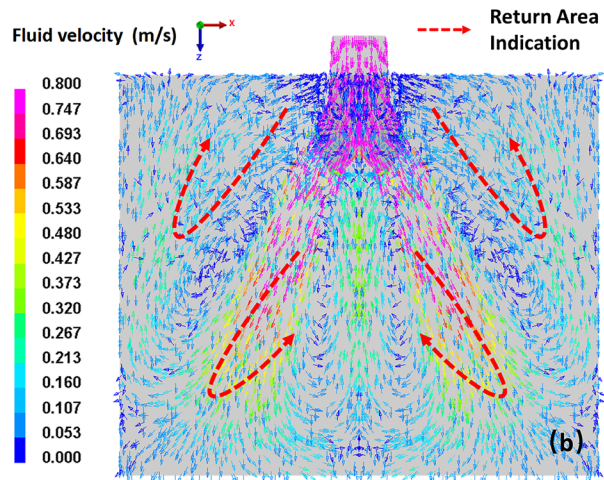
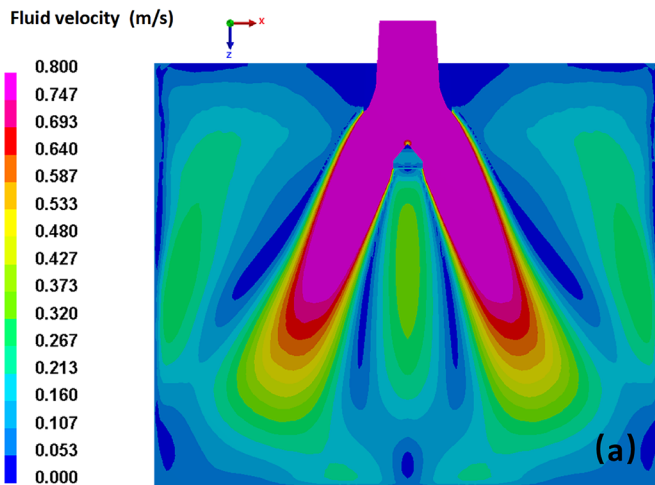


Fig. 10—Fluid velocity distribution in the mold for (a) cloud distribution and (b) flow direction.

IV. DISCUSSION

A. Factors of Influencing the Carbonizing from Mold flux to Liquid Steel

Generally, the mold flux will form the typical three-layer structure, including a granular mold flux layer, a sinter mold flux layer, and a molten mold flux, when the mold flux contacts the high-temperature liquid steel. Obviously, it is inevitable that the mold flux was not melted completely in time at the initial stage, and a small part of the carbon in the granular mold flux diffused into the liquid steel. Besides, a part of the carbon is oxidized and a very small part of the carbon is dissolved in the molten mold flux layer, and most of the remaining carbon will float to the vicinity of the sinter mold flux layer to form a carbon-rich layer.

On the one hand, when the mold flux forms a molten mold flux layer directly contacting liquid steel, the tendency of carbonizing is caused by the gradient of carbon concentration between liquid steel and molten mold flux. Hence, excessively high-carbon concentration in the molten mold flux layer will lead to the carbonizing phenomenon of ultra-low-carbon liquid steel, and the carbon concentration of the molten mold flux layer determines the upper limit of carbon concentration for carbonizing steel. On the other hand, when the liquid level of liquid steel fluctuates, the thickness of the molten mold flux layer of high-carbon slag is thinner, which may cause the carbon in carbon-rich layers, even sinter and granular layers, to easily be drawn into the liquid steel.

Obviously, the fluctuations in the liquid level make it possible for carbonizing the liquid steel, and the carbon concentration of the carbon-rich layer, the sinter mold flux layer, and the granular mold flux layer determines the carbonizing extent of the liquid steel. On the one hand, the trough position of the violently fluctuating may form grooves, which cause the carbon-rich layer or even sinter and granular layer to be drawn into the steel liquid. On the one hand, the peak position of the violently fluctuating may break through the molten mold flux layer, which causes the carbon-rich layer or even sinter and granular layer to directly contact the steel liquid.

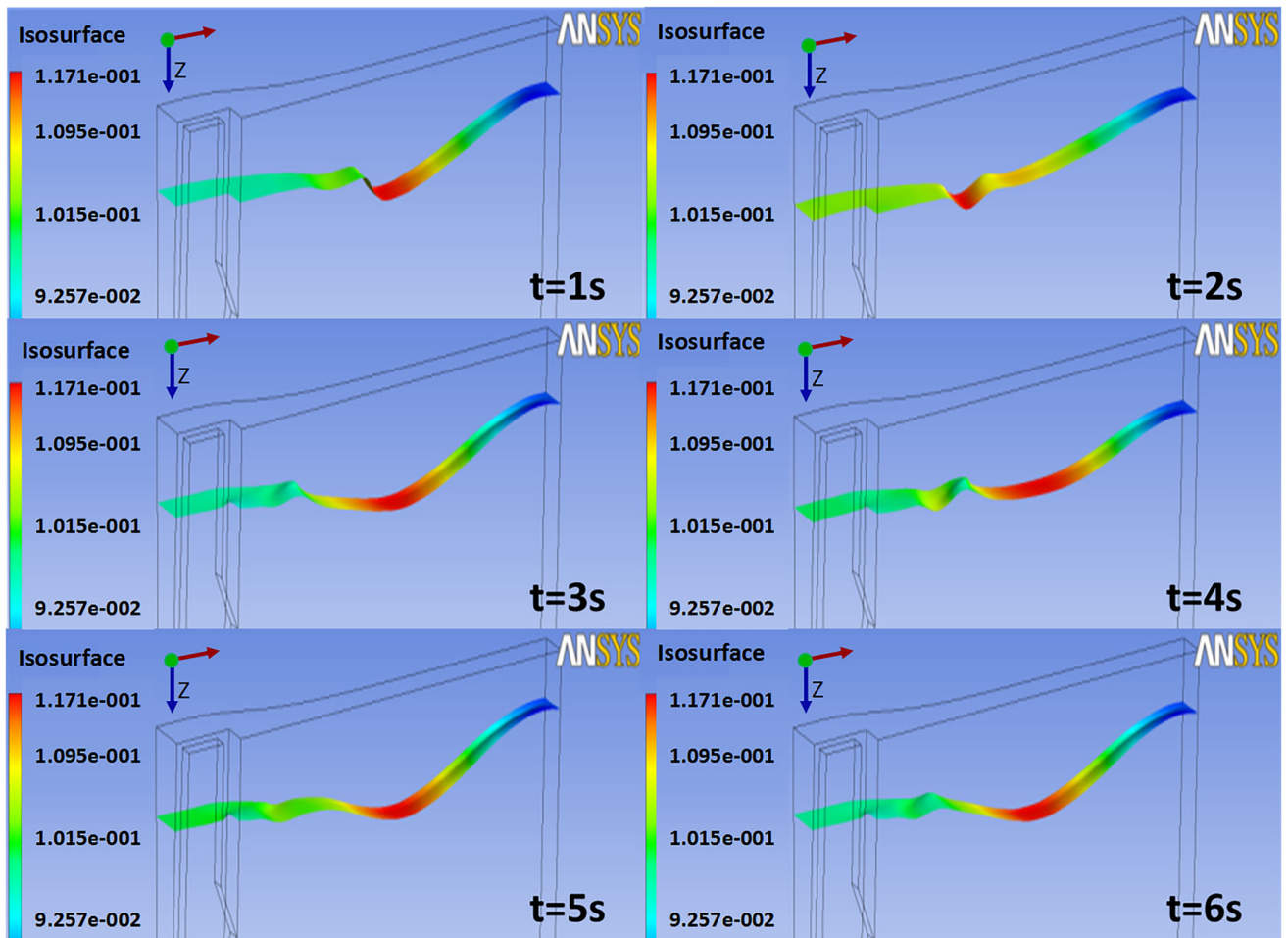


Fig. 11—Fluctuation of liquid steel free surface at different times.

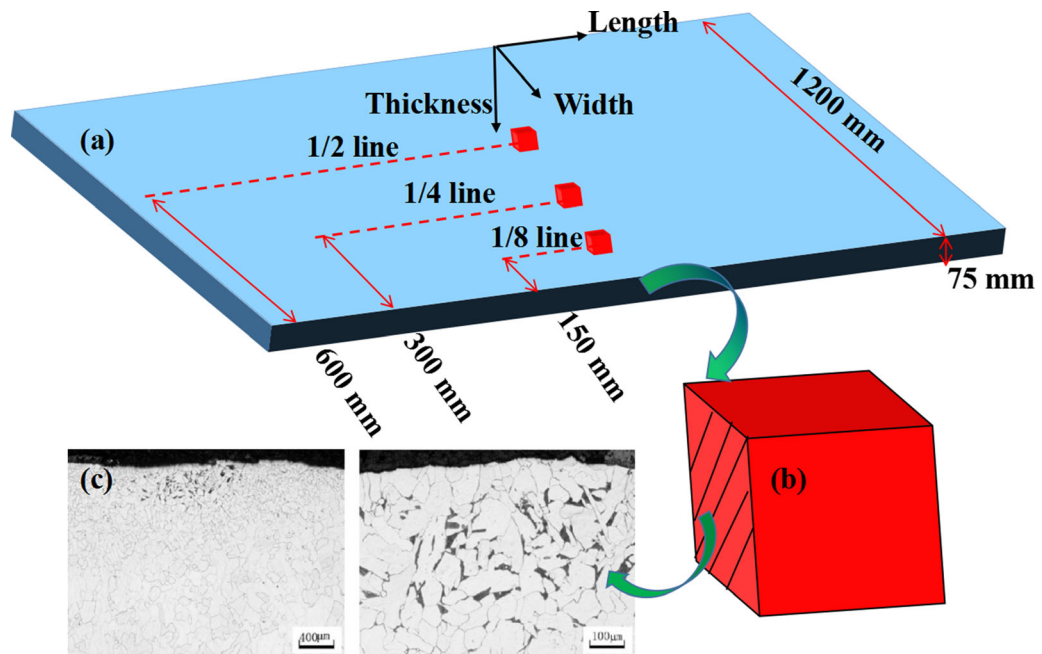


Fig. 12—Analysis of the carbonizing microstructure of a thin slab for (a) sampling position for thin slab, (b) microscopic observation section, and (c) typical carbonizing metallographic structure.

Obviously, both would significantly increase the carbon concentration gradient between the mold flux and liquid steel. The carbonizing phenomenon in ultra-low-carbon steel is unavoidable according to the two-phase carbon concentration difference at high temperatures.

B. Carbonizing Mechanism from Mold Flux to Liquid Steel

From the above-mentioned factors that influence the carbonizing from mold flux to liquid steel, there are only two possibilities. The dissolved carbon in the molten mold flux diffuses into the ultra-low-carbon liquid steel as shown in Figure 13(a), and the carbon of carbon-rich layer, sinter mold flux, and granular mold flux are drawn into the liquid steel accompanying liquid steel free surface fluctuations as shown in Figure 13(b), leading to the carbonizing of liquid steel.

Figure 13(a) shows the whole process regarding carbon in the molten mold flux diffusing into the ultra-low-carbon liquid steel (double-film theory).^[24,25] It is assumed that there is a stable phase interface between the molten mold flux and the liquid steel, and there are two thin stagnant films, which of thickness are δ_1 (nearing molten mold flux) and δ_2 (nearing liquid steel) on both sides of the interface. Additionally, the diffusion coefficients in molten mold flux and liquid steel are β_1 and β_2 , respectively; the carbon concentrations in molten mold flux and liquid steel are C_1 and C_2 , respectively; and the equilibrium carbon concentrations at the phase interface are C_{1^*} and C_{2^*} , respectively. Therefore, the diffusion rate of carbon in mold flux and liquid steel can be expressed as Eqs. [1] and [2], respectively.^[25]

$$J_1 = \frac{dn}{dt} = \beta_1(C_1 - C_{1^*})A, \quad [1]$$

$$J_2 = \frac{dn}{dt} = \beta_2(C_{2^*} - C_2)A, \quad [2]$$

where J_1 and J_2 are the diffusion rates of carbon in molten mold flux and liquid steel, respectively, the A is the contact area between liquid steel and molten mold flux. Additionally, the carbon dissolving process at the phase interface can be expressed as the following Eq. [3].

$$r = \frac{dn}{dt} = k(C_{1^*} - C_{2^*}), \quad [3]$$

where r and k are, respectively, the diffusion rate and diffusion coefficient of the phase interface. At high temperature, $k \gg \beta$ (β_1, β_2), it only needs to consider the diffusion rate in molten mold flux and liquid steel. From the double-film theory, $1/k = 0$, the total diffusion rate from molten mold flux to liquid can be expressed as Eq. [4].

$$r_T = \frac{1}{A} \frac{dn}{dt} = \frac{C_1 - C_2/L}{1/\beta_1 - 1/L\beta_2}. \quad [4]$$

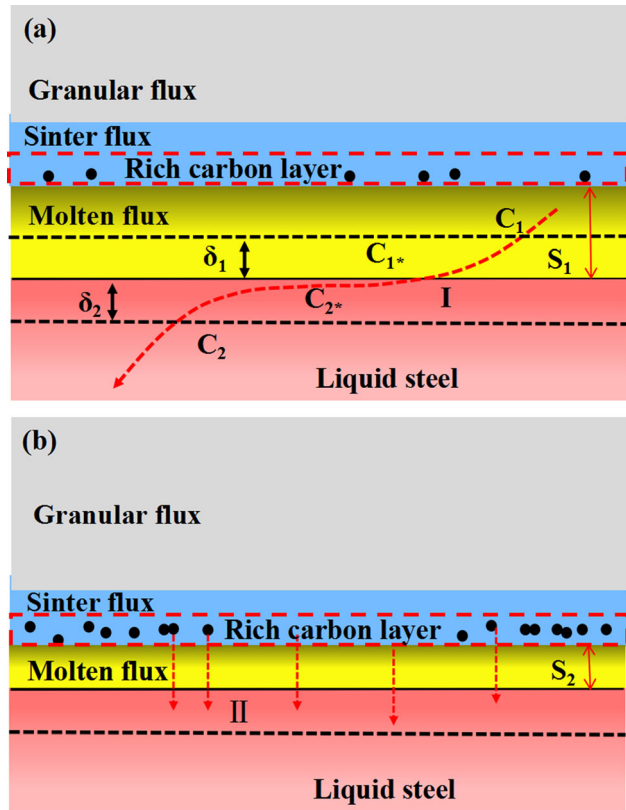


Fig. 13—Mechanism of carbonizing for (a) diffusion under steel liquid steady state and (b) mold flux drawn into steel liquid unstable state.

Generally, the diffusion coefficient of carbon in molten mold flux is much smaller than that in liquid steel, that is $L\beta_2 \gg \beta_1$. Hence, the limiting step is the diffusion of carbon in the molten mold flux, and the amount of diffusion of carbon can be expressed as Eq. [5]. Obviously, the diffusion amount of carbon is proportional to the carbon concentration in the molten mold flux and the diffusion coefficient. Therefore, the carbon in molten mold flux is inevitable diffusing to liquid steel owing to the carbon concentration gradient as shown in Table III.^[24]

$$Q = Ar_T = \frac{ab\beta_1\{\rho_s(C_1) - \rho_m[C_2]/L\}}{100M_C}. \quad [5]$$

Generally, the diffusion of carbon from the molten mold flux–steel interface to the interior of liquid steel can be regarded as unsteady diffusion in a semi-infinite medium. It is assumed that the carbon concentration in molten mold flux is C_i and the carbon concentration in liquid steel is C_0 . Hence, the carbon concentration $C(x, t)$ with the diffusion time (t) and distance (x) from the molten mold flux–steel interface to the interior of liquid steel can be obtained as Eq. [6].

$$C(x, t) = C_0 + (C_i - C_0)\left[1 - \operatorname{erf}\left(\frac{x}{2\sqrt{\beta_2 \cdot t}}\right)\right]. \quad [6]$$

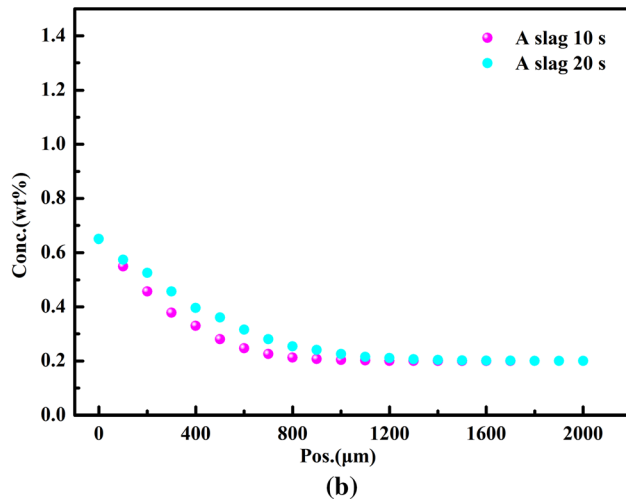
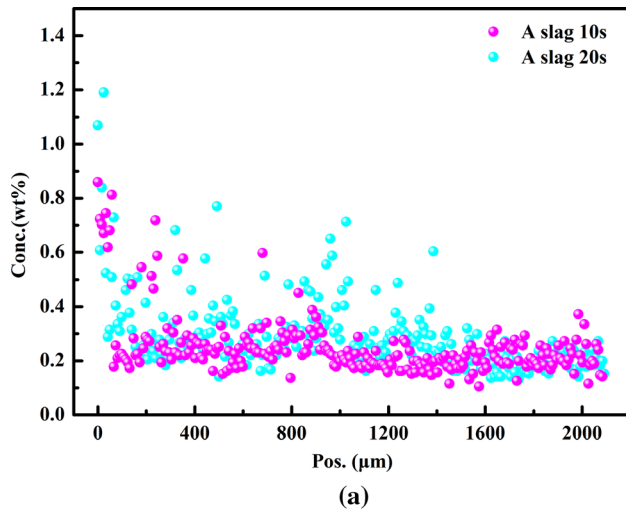


Fig. 14—Carbon concentration distribution from A slag–steel interface to the interior of steel after carbonizing with liquid steel holding temperature time for 10 and 20 seconds for (a) measured by EPMA and (b) calculated by regarded carbon diffusion in semi-infinite medium.

Generally, the diffusion coefficient of carbon in liquid steel (β_2) is $6.8 \times 10^{-9} \text{ m}^2/\text{s}$.^[26] According to the carbon concentration of molten mold flux and steel measured by EPMA, the carbon concentration in molten mold flux C_i is approximately 0.68 pct and the carbon concentration in liquid steel C_0 is approximately 0.20 pct. Hence, the carbon concentration distribution can be calculated by referencing the error function table.^[27] Figure 14 shows the measured carbon concentration distribution and calculated carbon concentration distribution from the A slag–steel interface to the interior of liquid steel after carbonizing with liquid steel holding temperature for 10 and 20 seconds. Obviously, the measured carbon concentration from Figure 14(a) is similar to the theoretical calculated results from Figure 14(b).

Additionally, it can be seen that the carbon concentration in the molten mold flux layer of low-carbon mold flux is higher as shown in Table III. However, high-carbon mold flux appears more carbonizing. Obviously, as shown in Figure 13(b), the carbon of carbon-rich layer, sinter mold flux, and granular mold flux are easily drawn into the liquid steel accompanied the liquid level fluctuations, which lead to the carbonizing of liquid steel. Especially, it leads to a more serious carbonizing phenomenon due to the thinner molten mold flux layer as well as the high-carbon concentration granular mold flux, sinter mold flux, and carbon-rich layer for the high-carbon mold flux.^[13,14] During the continuous casting process, the free surface fluctuation of liquid steel is also inevitable. It well reproduces the carbonizing phenomenon of mold flux during the continuous casting process.

V. CONCLUSIONS

- (1) When the ultra-low-carbon liquid steel contacts the carbon-containing mold flux, the micro-metallographic structure changes in the steel are from ferritic to chain pearlite and then flake pearlite with the increase of the liquid steel holding temperature time, and the chain pearlite originates from the grain boundaries of ferritic and grows up to form flake pearlite.
- (2) With the increase of the liquid steel holding temperature time, the amount of liquid steel carbonizing is more higher, and the high-carbon mold flux carbonizing is more faster than the low-carbon mold flux in the liquid steel. When the liquid steel of contacting low-carbon mold flux for holding temperature time is 10 to 20 seconds, respectively, the thickness of steel carbonizing is about 800 and 1500 μm , respectively. However, the steel samples with a thickness of 4000 μm have been completely carbonized when the liquid steel contacts the high-carbon mold flux for a holding temperature time of 20 seconds, which is containing high-carbon-rich layer. Even sinter and granular layers are easily entered into the unsteady fluctuation of liquid steel owing to the thinner molten mold flux.
- (3) For simulation, the carbonizing of mold flux during the continuous casting process is accidental, and high probability carbonizing is likely to occur at a quarter of the width in the thin slab continuous casting process due to the liquid surface fluctuations, which is consistent with the locations of carbonizing found in actual production sampling.

Therefore, it is suggested that reducing the carbon concentration of the molten mold flux layer, reducing the carbon concentration of the carbon-rich layer, appropriately increasing the thickness of the molten

layer, and reducing the fluctuation of the liquid steel level during the continuous casting process are effective ways to reduce the carbonizing of the liquid steel.

ACKNOWLEDGMENTS

This work is supported by the National Key Research and Development Program of China (No. 2021YFB3702401). The financial support from the Hunan Scientific Technology Projects (2020WK2003), and the National Science Foundation of China (52130408) is greatly acknowledged.

CONFLICT OF INTEREST

The authors declare that they have no known competing financial interests or personal relationships that could have appeared to influence the work reported in this paper.

REFERENCES

1. A. Srivastava and K. Chattopadhyay: *Metall. Mater. Trans. B*, 2022, vol. 53B, pp. 1018–35.
2. L.U. Yan-Qing, G.D. Zhang, M.F. Jiang, H.X. Liu, and L.I. Ting: *Steelmaking*, 2010, vol. 26, pp. 49–52.
3. C.J. Liu, Y.S. Wang, and Y.X. Zhu: *J. Iron Steel Res.*, 2000, vol. 12, pp. 46–50.
4. X.D. Wang, L.W. Kong, D.U. Feng-Ming, Y. Liu, X.Y. Zhang, and M. Yan: *ISIJ Int.*, 2015, vol. 54, pp. 2806–12.
5. J.W. Cho, T. Emi, H. Shibata, and M. Suzuki: *ISIJ Int.*, 1998, vol. 38, pp. 834–42.
6. R.B. Mahapatra, J.K. Brimacombe, and I.V. Samarasekera: *Metall. Mater. Trans. B*, 1991, vol. 22B, pp. 875–88.
7. J.J. Zhang, B.Y. Zhai, L. Zhang, and W.L. Wang: *J. Iron Steel Res. Int.*, 2022, <https://doi.org/10.1007/s42243-021-00714-y>.
8. E.F. Wei, Y.D. Yang, C.L. Feng, I.D. Sommerville, and A. McLean: *J. Iron Steel Res.*, 2006, vol. 2, pp. 22–26.
9. H. Wang: *J. Iron Steel Res.*, 2010, vol. 22, pp. 17–21.

10. A. Kamaraj, N. Haldar, P. Murugaiyan, and S. Misra: *Trans. Ind. Inst. Met.*, 2020, vol. 73, pp. 2025–31.
11. A. Kamaraj, A. Dash, P. Murugaiyan, and S. Misra: *Metall. Mater. Trans. B*, 2020, vol. 51B, pp. 2159–70.
12. Z.M. Yi, J.L. Song, and Q.C. Peng: *2013 World Congress in Materials Applications and Products Technology, 2013*, 2013, pp. 226–29.
13. J. Wu and Z.Q. Liu: *J. Baotou Univ. Iron Steel Technol.*, 2004, vol. 4, pp. 307–10 (in Chinese).
14. Z.L. Lei, D.D. Zhang, F. Me, and H.H. Zhao: *Contin. Cast.*, 2018, vol. 43, pp. 49–53.
15. M.B. Goldschmit, S.P. Ferro, and A. Owen: *Prog. Comput. Fluid Dyn. Int. J.*, 2004, vol. 4, p. 12.
16. Y.B. Liu, J. Yang, C. Ma, T. Zhang, F.B. Gao, T.-Q. Li, and J.L. Chen: *J. Iron Steel Res. Int.*, 2022, vol. 29, p. 17.
17. M. Bielnicki and J. Jowska: *Steel Res. Int.*, 2018, vol. 89, p. 1800110.
18. Z. Chen, W.T. Du, M. Zhang, Q. Wang, and S.P. He: *ISIJ Int.*, 2021, vol. 61, pp. 814–23.
19. F.A. Calvo, F. Molleda, J.M.G. de Salazar, A.J. Criado, and J.C. Suárez: *Metallography*, 1986, vol. 19, pp. 177–86.
20. Y.J. Zhang, G. Miyamoto, K. Shinbo, and T. Furuwara: *Acta Mater.*, 2020, vol. 186, pp. 533–44.
21. L.S. Zhang, X.F. Zhang, B. Wang, Q. Liu, and Z.G. Hu: *Metall. Mater. Trans. B*, 2014, vol. 45B, pp. 295–306.
22. K. Dou, E. Lordan, Y.J. Zhang, A. Jacot, and Z.Y. Fan: *Metall. Mater. Trans. A*, 2022, vol. 53A, pp. 3110–24.
23. K. Dou, E. Lordan, Y. Zhang, A. Jacot, and Z. Fan: *J. Mater. Process. Technol.*, 2021, vol. 296, p. 117193.
24. G.W. Lin, J. Wu, and Z.B. Li: *Spec. Steel*, 1999, vol. 20, pp. 13–16 (in Chinese).
25. J. Wu, Z.B. Li, and G.W. Lin: *Iron Steel*, 2000, vol. 35, pp. 17–19 (in Chinese).
26. M. Kosaka and S. Minowa: *Tetsu-to-Hagane*, 2010, vol. 53, pp. 983–97.
27. J.M. Coulson, J.F. Richardson, J.R. Backhurst, and H.J. Harker: *Chem. Eng. Sci.*, 1992, vol. 47, pp. 513–14.

Publisher's Note Springer Nature remains neutral with regard to jurisdictional claims in published maps and institutional affiliations.

Springer Nature or its licensor (e.g. a society or other partner) holds exclusive rights to this article under a publishing agreement with the author(s) or other rightsholder(s); author self-archiving of the accepted manuscript version of this article is solely governed by the terms of such publishing agreement and applicable law.